

REPORT DOCUMENTATION PAGE			Form Approved OMB NO. 0704-0188		
<p>The public reporting burden for this collection of information is estimated to average 1 hour per response, including the time for reviewing instructions, searching existing data sources, gathering and maintaining the data needed, and completing and reviewing the collection of information. Send comments regarding this burden estimate or any other aspect of this collection of information, including suggestions for reducing this burden, to Washington Headquarters Services, Directorate for Information Operations and Reports, 1215 Jefferson Davis Highway, Suite 1204, Arlington VA, 22202-4302. Respondents should be aware that notwithstanding any other provision of law, no person shall be subject to any penalty for failing to comply with a collection of information if it does not display a currently valid OMB control number. PLEASE DO NOT RETURN YOUR FORM TO THE ABOVE ADDRESS.</p>					
1. REPORT DATE (DD-MM-YYYY) 18-11-2019		2. REPORT TYPE Final Report		3. DATES COVERED (From - To) 15-Aug-2014 - 14-Aug-2015	
4. TITLE AND SUBTITLE Final Report: Scanning Probe Microscope for Polymeric and Hybrid Materials Research and Education			5a. CONTRACT NUMBER W911NF-14-1-0450		
			5b. GRANT NUMBER		
			5c. PROGRAM ELEMENT NUMBER 611103		
6. AUTHORS			5d. PROJECT NUMBER		
			5e. TASK NUMBER		
			5f. WORK UNIT NUMBER		
7. PERFORMING ORGANIZATION NAMES AND ADDRESSES Drexel University Office of Research 3201 Arch Street, Suite 100 Philadelphia, PA 19104 -2875			8. PERFORMING ORGANIZATION REPORT NUMBER		
9. SPONSORING/MONITORING AGENCY NAME(S) AND ADDRESS (ES) U.S. Army Research Office P.O. Box 12211 Research Triangle Park, NC 27709-2211			10. SPONSOR/MONITOR'S ACRONYM(S) ARO		
			11. SPONSOR/MONITOR'S REPORT NUMBER(S) 65106-CH-RIP.1		
12. DISTRIBUTION AVAILABILITY STATEMENT Approved for public release; distribution is unlimited.					
13. SUPPLEMENTARY NOTES The views, opinions and/or findings contained in this report are those of the author(s) and should not be construed as an official Department of the Army position, policy or decision, unless so designated by other documentation.					
14. ABSTRACT					
15. SUBJECT TERMS					
16. SECURITY CLASSIFICATION OF:			17. LIMITATION OF ABSTRACT UU	15. NUMBER OF PAGES	19a. NAME OF RESPONSIBLE PERSON Giuseppe Palmese
a. REPORT UU	b. ABSTRACT UU	c. THIS PAGE UU			19b. TELEPHONE NUMBER 215-895-5814

RPPR Final Report

as of 11-Dec-2019

Agency Code:

Proposal Number: 65106CHRIP

Agreement Number: W911NF-14-1-0450

INVESTIGATOR(S):

Name: Chris Li
Email: cyl24@drexel.edu
Phone Number: 2158952082
Principal: N

Name: Giuseppe Palmese palmese@co
Email: grp27@drexel.edu
Phone Number: 2158955814
Principal: Y

Organization: **Drexel University**

Address: Office of Research, Philadelphia, PA 191042875

Country: USA

DUNS Number: 002604817

EIN: 231352630

Report Date: 14-Nov-2015

Date Received: 18-Nov-2019

Final Report for Period Beginning 15-Aug-2014 and Ending 14-Aug-2015

Title: Scanning Probe Microscope for Polymeric and Hybrid Materials Research and Education

Begin Performance Period: 15-Aug-2014

End Performance Period: 14-Aug-2015

Report Term: 0-Other

Submitted By: Giuseppe Palmese

Email: grp27@drexel.edu

Phone: (215) 895-5814

Distribution Statement: 1-Approved for public release; distribution is unlimited.

STEM Degrees:

STEM Participants:

Major Goals: Under this award, we have purchase a scanning probe microscope (SPM) for polymeric and hybrid materials research and education at Drexel University. The instrument is fully operational and is housed by itself in a small quiet room in the Lebow building of Drexel's College of Engineering.

Accomplishments: Under this award, we have purchase a scanning probe microscope (SPM) for polymeric and hybrid materials research and education at Drexel University. The instrument is fully operational and is housed by itself in a small quiet room in the Lebow building of Drexel's College of Engineering. The chosen model is the Multimode® 8 SPM (Bruker) combined with state-of-the-art low-noise, high-bandwidth NanoScope® V control station, which allows for ultra-high resolution imaging modes (e.g., ScanAsyst®) as shown in Figure 1. A number of standard scanning modes are included with this instrument: tapping mode, contact mode, and non-contact mode. In addition, the SPM also includes a few specific advanced modes:

1. **Phase Imaging:** Phase imaging is a secondary imaging mode derived from tapping mode that goes beyond topographical data to detect variations in composition, adhesion, friction, viscoelasticity, and other properties, including electric and magnetic. It is the mapping of the phase lag between the periodic signal that drives the cantilever and the oscillations of the cantilever.
2. **Lateral Force Microscopy (LFM):** LFM is a secondary contact AFM mode that detects and maps relative differences in the frictional forces between the probe tip and the sample surface. In LFM, the scanning is always perpendicular to the long axis of the cantilever. Forces on the cantilever that are parallel to the plane of the sample surface cause twisting of the cantilever around its long axis. This twisting is measured by a quad-cell, position-sensitive photo detector.
3. **Scanning Tunneling Microscopy (STM):** As previously mentioned, STM measures topography of surface electronic states using a tunneling current that is dependent on the separation between the probe tip and a sample surface. [30]
4. **Tunneling AFM (TUNA):** TUNA works similarly to Conductive AFM, but with higher sensitivities (ultra low

RPPR Final Report as of 11-Dec-2019

currents (<1 pA) through the thickness of thin films). The TUNA application module can operate in imaging or spectroscopy mode. TUNA can operate as a secondary imaging mode derived from contact AFM that characterizes conductivity variations across medium- to low-conducting and semiconducting materials. TUNA employs a conductive probe tip. Typically, a DC bias is applied to the tip, and the sample is held at ground potential. While the z-feedback signal is used to generate a normal contact AFM topography image, the current passing between the tip and sample is measured to generate the conductive AFM image.

5. Environmental Control: In situ observation of polymer morphology under different environments is critical for understanding their structure and formation mechanisms. A single controller that controls sample temperature and humidity from -35°C to 250°C and 0 to 100% RH, respectively, has been included in the proposed instrument to allow for in situ experiments.

6. Fluid Imaging Cells: Fluid imaging cells provide contact mode and tapping mode AFM imaging in fluid environments. A cell consists of a glass cantilever holder and silicon o-ring to form an enclosed fluid environment with the ability to exchange liquids. Tapping mode can be conducted by oscillating the cantilever acoustically or by magnetic actuated drive.

Results from the newly acquired SPM.

Janus polymer crystals (Li): In our recent work, we created an oil/water interface where crystalline dicarboxyl end-functionalized PCL (COOH-PCL-COOH, Mn=7200, 2500 g/mol) is dissolved in the oil phase, evaporation of which induces PCL crystallization. Millimeter scale uniform PCL lamellae are formed with the carboxyl end groups pinned at the water surface, which breaks the centrosymmetry of the PCL lamella, leading to Janus PSC nanosheets. Figure 2a shows the evaporative crystallization process of COOH-PCL-COOH at water/pentyl acetate interface. In the experiment, PCL/1-butanol solution with a concentration of 0.03 wt. % was prepared at 60 °C and was subsequently cooled to -10 °C for 2 hrs. The solution was then brought to 44.5 °C for 10 min to produce polymer seeds. A 200ul of the as prepared polymer seed solution was drop-wisely transferred to a pentyl acetate/water biphasic solution with 1g pentyl acetate covering the water surface, as shown in Figure 2a. The evaporative crystallization occurred at ambient temperature for approximately 4 days, when the organic solvent evaporated and a polymer film was formed. COOH-PCL-COOH can be seen as an amphiphile with its hydrophobic backbone and hydrophilic carboxyl end groups. Upon crystallization, we envisage that COOH groups will be pinned at the water surface, and noncentrosymmetric PCL single crystals can be obtained (Figure 1a).

Figure 2b shows a phase-contrast optical microscopy image of the resultant quasi 2D PCL nanosheet. Part I in the image refers to the background; part II is the PSC sheet, and the inset shows the PCL single crystal with clear facets. The red line annotated angle is 125°, corresponding to the angle between {110} and {100} faces of PCL. The grey elongated rods on top of the PSC sheet appear to be overgrown PCL crystals, probably due to excess polymers added. Of interest is that all the long axes of the rods are parallel with each other. Based on PCL single crystal structure and morphology, the long axis of the rods represents PCL crystal b-axis, and the uniform alignment of these b-axes suggest that, disregarding the fold surface of the PCL crystals, these overgrowth follows an epitaxial growth mechanism with the substrate, and more importantly, the underlying PSC nanosheet is a single crystal with a uniform crystal orientation.

The crystal structure of the PCL nanosheet can be confirmed using selected area electron diffraction (SAED) experiments, as shown in Figure 3a. The SAED pattern is consistent with the reported PCL orthorhombic unit cell, $a=0.748\text{nm}$, $b=0.498\text{nm}$, and $c=1.726\text{nm}$. Only (hk0) diffraction planes are observed, indicating that the c-axis, and the polymer chain is perpendicular to the PSC nanosheet. The overall thickness of the PSC sheet is measured to be about 9 nanometer using atomic force microscopy (AFM, Figure 3b). Considering the PCL unit cell parameters and the molecular weight of PCL, we can conclude that a single COOH-PCL-COOH chain folds 5 times along the direction perpendicular to the film surface (Figure 3d). In comparison, our control experiment shows that the COOH-PCL-COOH PSC crystallized in solution under the same condition is 7.7nm thick, which corresponds to 6-time folding. As shown in Figure 2d, 6-time folding of the PCL chain leads to a symmetric lamella, which the chain ends evenly distributed on both surfaces of the lamella. At the water/pentyl acetate interface, all carboxyl groups are pinned at the water surface during crystallization, and such a chain conformation is incommensurate with 6-time folding. Consequently, 5-time folding was formed in the evaporative crystallization case where the lamellar thickness increased from 7.7 to 9 nanometer. We further used 2.5 K g/mol COOH-PCL-COOH to conduct similar experiments. As shown in Figure 2e, f, the polymer chains fold two and three times when crystallize in solution, or

RPPR Final Report as of 11-Dec-2019

at the interface, respectively. This is consistent with our results using 7.2 K g/mol PCL.

It has been a challenging task to confirm the Janus nature of nanoparticles, particularly when the length scale is sub-20 nanometer. Typically, staining is used for microscopy experiments, while contrast has been an issue in many cases. In the present work, we validated the Janus property of our PSC nanosheets by measuring water contact angles on each side using in-situ water condensation under ESEM. In-situ condensation, instead of sessile drop, was used to better reveal the local wettability information with small water droplets (40~100um in diameter). Detailed experimental condition and data analysis can be found in supporting information. In brief, a sample was mounted to a 60 d

Training Opportunities: Nothing to Report

Results Dissemination: Nothing to Report

Honors and Awards: Nothing to Report

Protocol Activity Status:

Technology Transfer: Nothing to Report

PARTICIPANTS:

Participant Type: Co PD/PI

Participant: Christopher Li

Person Months Worked: 1.00

Project Contribution:

International Collaboration:

International Travel:

National Academy Member: N

Other Collaborators:

Funding Support:

Participant Type: PD/PI

Participant: Giuseppe R. Palmese

Person Months Worked: 1.00

Project Contribution:

International Collaboration:

International Travel:

National Academy Member: N

Other Collaborators:

Funding Support:

REPORT DOCUMENTATION PAGE

*Form Approved
OMB No. 0704-0188*

The public reporting burden for this collection of information is estimated to average 1 hour per response, including the time for reviewing instructions, searching existing data sources, gathering and maintaining the data needed, and completing and reviewing the collection of information. Send comments regarding this burden estimate or any other aspect of this collection of information, including suggestions for reducing the burden, to Department of Defense, Washington Headquarters Services, Directorate for Information Operations and Reports (0704-0188), 1215 Jefferson Davis Highway, Suite 1204, Arlington, VA 22202-4302. Respondents should be aware that notwithstanding any other provision of law, no person shall be subject to any penalty for failing to comply with a collection of information if it does not display a currently valid OMB control number.

PLEASE DO NOT RETURN YOUR FORM TO THE ABOVE ADDRESS.

1. REPORT DATE (DD-MM-YYYY) 14-07-2016	2. REPORT TYPE Final	3. DATES COVERED (From - To) 15/08/2014- 14/08/2015
---	-------------------------	--

4. TITLE AND SUBTITLE ScanningProbeMicroscopefor PolymericandHybrid MaterialsResearchand Education	5a. CONTRACT NUMBER W911NF-14-1-0450
	5b. GRANT NUMBER
	5c. PROGRAM ELEMENT NUMBER

6. AUTHOR(S) GiuseppePalmeseandChristopheLi, DrexelUniversity	5d. PROJECT NUMBER
	5e. TASK NUMBER
	5f. WORK UNIT NUMBER

7. PERFORMING ORGANIZATION NAME(S) AND ADDRESS(ES) DrexelUniversity 1505RaceStreet,10thFloor PhiladelphiaPA 19102-1119	8. PERFORMING ORGANIZATION REPORT NUMBER
---	--

9. SPONSORING/MONITORING AGENCY NAME(S) AND ADDRESS(ES) Departmentof Defense	10. SPONSOR/MONITOR'S ACRONYM(S) DoD
	11. SPONSOR/MONITOR'S REPORT NUMBER(S)

12. DISTRIBUTION/AVAILABILITY STATEMENT

13. SUPPLEMENTARY NOTES

14. ABSTRACT

Underthis award,we havepurchasea scanningprobemicroscope(SPM)for polymericandhybrid materialsresearchandeducation atDrexelUniversity. Thechosedmodelis the MultimodeAFM SPM(Bruker)combinedwith state-of-the-artlow-noise, high-bandwidthNanoScopeAFM controlstation,which allowsfor ultra-highresolutionimagingmodes(e.g., ScanAsystAFM)as shown in Figure1. TheSPMincludea numberof standardscanningmodesincluding in theproposednstrument,includingtappingmode, contactmode,andnon-contactmode.

15. SUBJECT TERMS

scanningprobemicroscopepolymers,composites

16. SECURITY CLASSIFICATION OF:			17. LIMITATION OF ABSTRACT	18. NUMBER OF PAGES	19a. NAME OF RESPONSIBLE PERSON
a. REPORT U	b. ABSTRACT U	c. THIS PAGE U			SAR

PROJECT FINAL REPORT

#W911NF-14-1-0450 (Scanning Probe Microscope for Polymeric and Hybrid Materials Research and Education)
15/08/2014 – 14/08/2015

Giuseppe Palmese and Christopher Li, Drexel University

Under this award, we have purchase a scanning probe microscope (SPM) for polymeric and hybrid materials research and education at Drexel University. The instrument is fully operational and is housed by itself in a small quiet room in the Lebow building of Drexel's College of Engineering. The chosen model is the **Multimode[®] 8 SPM** (Bruker) combined with state-of-the-art low-noise, high-bandwidth NanoScope[®] V control station, which allows for ultra-high resolution imaging modes (e.g., ScanAsyst[®]) as shown in **Figure 1**. A number of standard scanning modes are included with this instrument: tapping mode, contact mode, and non-contact mode. In addition, the SPM also includes a few specific advanced modes:

1. **Phase Imaging:** Phase imaging is a secondary imaging mode derived from tapping mode that goes beyond topographical data to detect variations in composition, adhesion, friction, viscoelasticity, and other properties, including electric and magnetic. It is the mapping of the phase lag between the periodic signal that drives the cantilever and the oscillations of the cantilever.
2. **Lateral Force Microscopy (LFM):** LFM is a secondary contact AFM mode that detects and maps relative differences in the frictional forces between the probe tip and the sample surface. In LFM, the scanning is always perpendicular to the long axis of the cantilever. Forces on the cantilever that are parallel to the plane of the sample surface cause twisting of the cantilever around its long axis. This twisting is measured by a quad-cell, position-sensitive photo detector.
3. **Scanning Tunneling Microscopy (STM):** As previously mentioned, STM measures topography of surface electronic states using a tunneling current that is dependent on the separation between the probe tip and a sample surface. [30]
4. **Tunneling AFM (TUNA):** TUNA works similarly to Conductive AFM, but with higher sensitivities (ultra low currents (<1 pA) through the thickness of thin films). The TUNA application module can operate in imaging or spectroscopy mode. TUNA can operate as a secondary imaging mode derived from contact AFM that characterizes conductivity variations across medium- to low-conducting and semiconducting materials. TUNA employs a conductive probe tip. Typically, a DC bias is applied to the



Figure 1. The proposed Bruker Multimode[®] 8 SPM with NanoScope[®] V control station.

tip, and the sample is held at ground potential. While the z-feedback signal is used to generate a normal contact AFM topography image, the current passing between the tip and sample is measured to generate the conductive AFM image.

5. **Environmental Control:** *In situ* observation of polymer morphology under different environments is critical for understanding their structure and formation mechanisms. A single controller that controls sample temperature and humidity from -35°C to 250°C and 0 to 100% RH, respectively, has been included in the proposed instrument to allow for *in situ* experiments.
6. **Fluid Imaging Cells:** Fluid imaging cells provide contact mode and tapping mode AFM imaging in fluid environments. A cell consists of a glass cantilever holder and silicon o-ring to form an enclosed fluid environment with the ability to exchange liquids. Tapping mode can be conducted by oscillating the cantilever acoustically or by magnetic actuated drive.

Results from the newly acquired SPM.

Janus polymer crystals (Li): In our recent work, we created an oil/water interface where crystalline dicarboxyl end-functionalized PCL (COOH-PCL-COOH, Mn=7200, 2500 g/mol) is dissolved in the oil phase, evaporation of which induces PCL crystallization. Millimeter scale uniform PCL lamellae are formed with the carboxyl end groups pinned at the water surface, which breaks the centrosymmetry of the PCL lamella, leading to Janus PSC nanosheets. Figure 2a shows the evaporative crystallization process of COOH-PCL-COOH at water/pentyl acetate interface. In the experiment, PCL/1-butanol solution with a concentration of 0.03 wt. % was prepared at 60 °C and was subsequently cooled to -10 °C for 2 hrs. The solution was then brought to 44.5 °C for 10 min to produce polymer seeds. A 200ul of the as prepared polymer seed solution was drop-wisely transferred to a pentyl acetate1/water biphasic solution with 1g pentyl acetate covering the water surface, as shown in Figure 2a. The evaporative crystallization occurred at ambient temperature for approximately 4 days, when the organic solvent evaporated and a polymer film was formed. COOH-PCL-COOH can be seen as an amphiphile with its hydrophobic backbone and hydrophilic carboxyl end groups. Upon crystallization, we envisage that COOH groups will be pinned at the water surface, and noncentrosymmetric PCL single crystals can be obtained (Figure 1a).

Figure 2b shows a phase-contrast optical microscopy image of the resultant quasi 2D PCL nanosheet. Part I in the image refers to the background; part II is the PSC sheet, and the inset shows the PCL single crystal with clear facets. The red line annotated angle is 125° , corresponding to the angle between $\{110\}$ and $\{100\}$ faces of PCL. The grey elongated rods on top of the PSC sheet appear to be overgrown PCL crystals, probably due to excess polymers added. Of interest is that all the long axes of the rods are parallel with each other. Based on PCL single crystal structure and morphology, the long axis of the rods represents PCL crystal b-axis, and the uniform alignment of these b-axes suggest that, disregarding the fold surface of the PCL crystals, these overgrowth follows an epitaxial growth mechanism with the substrate, and more importantly, the underlying PSC nanosheet is a single crystal with a uniform crystal orientation.

The crystal structure of the PCL nanosheet can be confirmed using selected area electron diffraction (SAED) experiments, as shown in Figure 3a. The SAED pattern is consistent with the reported PCL orthorhombic unit cell, $a=0.748\text{nm}$, $b=0.498\text{nm}$, and $c=1.726\text{nm}$. Only $(hk0)$ diffraction planes are observed, indicating that the c -axis, and the polymer chain is perpendicular to the PSC nanosheet. The overall thickness of the PSC sheet is measured to be about 9 nanometer using atomic force microscopy (AFM, Figure 3b). Considering the PCL unit cell parameters and the molecular weight of PCL, we can conclude that a single COOH-PCL-COOH chain folds 5 times along the direction perpendicular to the film surface (Figure 3d). In comparison, our control experiment shows that the COOH-PCL-COOH PSC crystallized in solution under the same condition is 7.7nm thick, which corresponds to 6-time folding. As shown in Figure 2d, 6-time folding of the PCL chain leads to a symmetric lamella, which the chain ends evenly distributed on both surfaces of the lamella. At the water/pentyl acetate interface, all carboxyl groups are pinned at the water surface during crystallization, and such a chain conformation is incommensurate with 6-time folding. Consequently, 5-time folding was formed in the evaporative crystallization case where the lamellar thickness increased from 7.7 to 9 nanometer. We further used 2.5 K g/mol COOH-PCL-COOH to conduct similar experiments. As shown in Figure 2e, f, the polymer chains fold two and three times when crystallize in solution, or at the interface, respectively. This is consistent with our results using 7.2 K g/mol PCL.

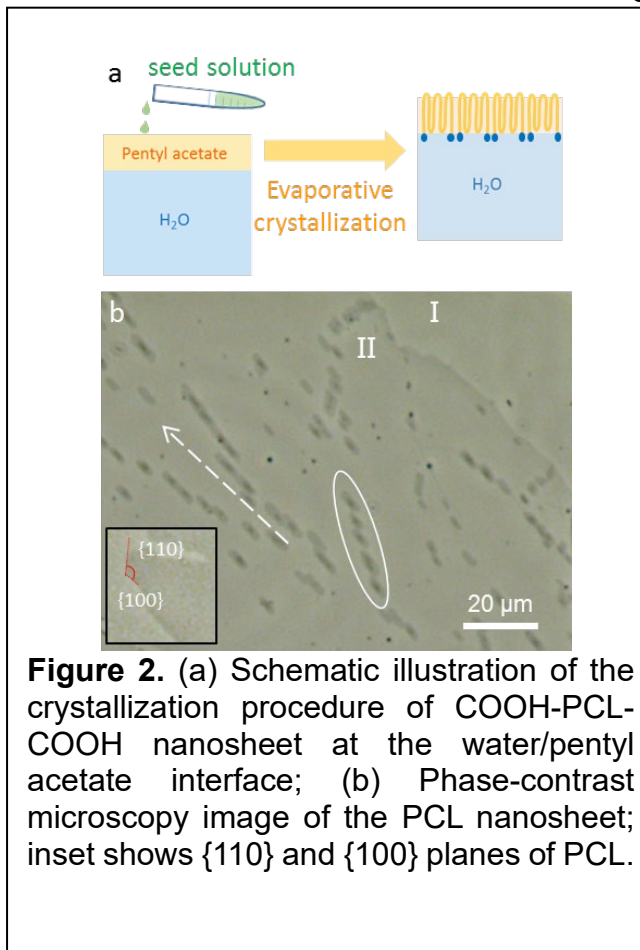


Figure 2. (a) Schematic illustration of the crystallization procedure of COOH-PCL-COOH nanosheet at the water/pentyl acetate interface; (b) Phase-contrast microscopy image of the PCL nanosheet; inset shows $\{110\}$ and $\{100\}$ planes of PCL.

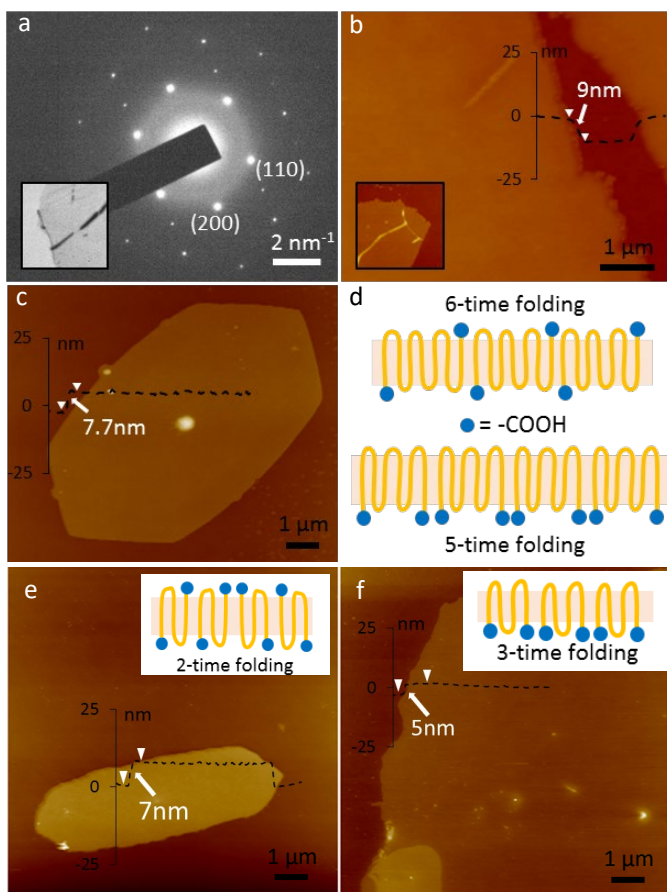
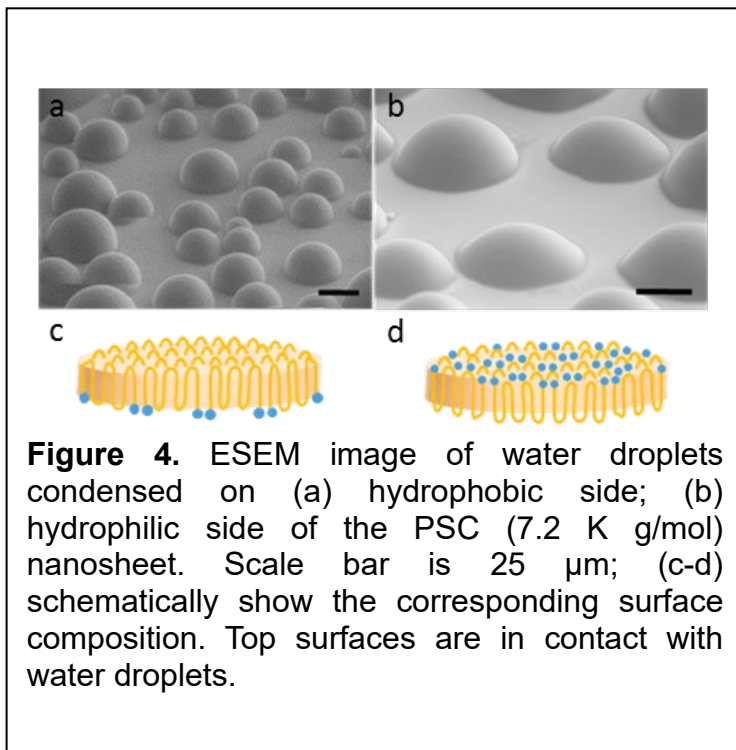


Figure 3. (a) Electron diffraction pattern of COOH-PCL-COOH single crystal film, inset: Transmission electron microscopy (TEM) image (horizontal field width = 11 μm); (b) Atomic force microscopy (AFM) images of COOH-PCL-COOH single crystal nanosheet and the corresponding height profile, inset: morphology of a PCL single crystal tip (horizontal field width = 2.5 μm). (c) AFM image of COOH-PCL-COOH single crystal prepared through solution crystallization and the corresponding height profile; (d) Side-views of COOH-PCL-COOH crystals showing the chain folding during solution crystallization (top) and evaporative crystallization (bottom). (a)-(d) represent PCL with a 7.2 K g/mol molecular weight. (e) and (f) show AFM images of COOH-PCL-COOH ($M_n=2.5\text{K g/mol}$) prepared from solution crystallization (e) and evaporative crystallization (f). Insets show side-view of corresponding chain folding.

It has been a challenging task to confirm the Janus nature of nanoparticles, particularly when the length scale is sub-20 nanometer. Typically, staining is used for microscopy experiments, while contrast has been an issue in many cases. In the present work, we validated the Janus property of our PCL nanosheets by measuring water contact angles on each side using in-situ water condensation under ESEM. In-situ condensation, instead of sessile drop, was used to better reveal the local wettability information with small water droplets (40~100 μm in diameter). Detailed experimental condition and data analysis can be found in supporting information. In brief, a sample was mounted to a 60 degree tilted stage. The Peltier cooler stage on the back of the sample was kept at 1 $^\circ\text{C}$ and the initial vapor pressure was 3 torr. To induce water condensation, the vapor pressure was slowly increased at the rate of 0.1 torr per 20s, until a condensation droplet is observed. Afterwards, the vapor pressure was kept constant and the droplets can be considered as in an

equilibrium state (negligible growth when the images were captured). Figure 4 shows the ESEM image of water droplets condensed on the PSC ($M_n = 7.2$ K g/mol) nanosheet surface that was facing the pentyl acetate (a) and water (b) phase during crystallization; and the calculated contact angles are $82 \pm 1^\circ$ (a) and $61 \pm 5^\circ$ (b), respectively (for detailed calculation, see supporting information). It is therefore evident that the contact angle of the two sides of the PSC nanosheets directly exhibits hydrophobicity difference. Meanwhile, the vapor pressure required to condense for both sides is different: 5.3 torr for the more hydrophobic side versus 4.9 torr for the more hydrophilic side, implying a higher energy barrier for water vapor to condense on the hydrophobic side. Thus, both the contact angle and vapor pressure measurements suggest the PSC film obtained from the evaporative crystallization is a Janus nanosheet.



In summary, we have fabricated Janus polymer single crystals using evaporative crystallization at water/pentyl acetate interface. Telechelic COOH-PCL-COOH crystallizes at water/pentyl acetate interface upon evaporation of pentyl acetate. Water phase pinned the hydrophilic chain ends, altered chain folding conformation, and led to a noncentrosymmetric Janus single crystal nanosheet. In-situ nanocondensation experiments quantitatively demonstrated the Janus nature of the nanosheets. We anticipate that our approach can be used to fabricate ordered Janus 2D materials with various sizes and functions.

Biobased rubber tougheners for epoxy thermosets (Palmese): In this work, a series of bio-rubber (BR) tougheners was prepared by grafting renewable fatty acids with different chain lengths onto ESO at varying molar ratios through an esterification reaction, providing prepared BRs with diverse MWs, functionalities and compatibilities with epoxy resins. Renewable acids, such as n-hexanoic acid, n-octanoic acid and n-decanoic acid, were used to make these BRs fully sustainable. Their successful preparations were verified and the toughening effect was investigated using commercial epoxy resin, DGEBA EPON 828 ($n = 0.13$), with an aromatic amine hardener, diethyl toluene diamine (EPIKURE W). Fracture toughness and thermomechanical properties of control and BR toughened samples were evaluated, and fracture surface morphology is investigated using scanning electron microscope (SEM) and atomic force microscope (AFM).

Secondary rubbery phases with tunable particle sizes depending on BR type and weight fraction were found to occur in cured networks and responsible for the fracture toughness enhancements. With other excellent advantages, such as low viscosity and cost, these BRs are demonstrated to be promising tougheners for thermosetting epoxy resins.

The fracture surface morphology of BR toughened samples was also investigated using the newly acquired AFM. Figure 5 displays three-dimension AFM images of selected phase-separated samples whose SEM images are also in Figure 5. As shown, fracture surfaces of these samples are embedded with crater-like architectures and holes with different sizes, indicating that rubbery particles are formed in cured networks. When a phase-separated sample is fractured at RT, rubbery particles together with the matrix are also fractured. However, since these particles are much tougher and covalently bonded with the matrix, they are unevenly fractured and result in either crater-like architectures or holes. The crater-like architectures are fractured particles sticking on the surfaces and the holes result from the rubbery particles being pulled out from the matrix in which particle residuals can be observed at the bottoms of the holes. In many cases there is clear evidence of cavitation and matrix shear yielding.

